Scaling laws and snap-through events in indentation of perforated membranes

Fei Jia, Martine Ben Amar

Scaling laws and Snap-through events in indentation of perforated membranes

Fei Jia[a], Martine Ben Amar[b,c,*]

[a] *Department of Astronautical Science and Mechanics, Harbin Institute of Technology (HIT), No.92 West Dazhi Street, 150001 Harbin, China*
[b] *Laboratoire de Physique de l'Ecole normale supérieure, ENS, Université PSL, CNRS, Sorbonne Université, 24 rue Lhomond, 75005 Paris, France*
[c] *Institut Universitaire de Cancérologie, Faculté de médecine, Université Pierre et Marie Curie-Paris 6, 91 Bd de l'Hôpital, 75013 Paris, France*

Abstract

We revisit the classical theory of indentation for very soft materials. Many experiments consist in extracting the stiffness of a membrane from the cubic answer of the force versus indentation depth. However, this law is restricted to a perfect membrane under a sharp point loading. In biophysical experiments, where this technique recovers some success at low scales thanks to AFM, the thin samples are highly deformable, hyperelastic, pre-stretched and often attached to a substrate which cannot be neglected. In addition microscopic tiny pores may exist or may be created by the indenter. This diversity requires specific studies with the correct elasticity: here we choose the Neo-Hookean elastic model at large membrane deformations. We show that, the weak loading regime is extremely sensitive to any physical properties of the thin layer but also of the indenter geometry. In addition, when a hole exists, at finite forcing or finite indentation depth, we discover a topological bifurcation with abrupt dynamical jump variation of typical quantities such as the hole size. This bifurcation is similar to the famous catenoid instabilities which are also due to a topological bifurcation, when the two rings of support are pulled apart. This bifurcation is robust in the sense that it always exists whatever the physical properties of the sample.

Keywords: non-linear elasticity, bifurcations, topological transitions, scaling laws

*Corresponding author
Email address: benamar@lps.ens.fr (Martine Ben Amar)

1. Introduction

The traditional indentation technique has recently recovered popularity in nanophysics [1, 2] and biophysics [3, 4]. In these two areas, mechanics mostly elasticity are coupled to other active fields and their role requires precise non-trivial measurements at low scales from nanometres to microns. In practice, this technique provides the stiffness μ of the samples by comparing the applied force F to the deflection amplitude δ, according to the law: $F/\mu \sim \delta^3$, which is assumed to be valid for thin membranes under weak forcing. However, as demonstrated recently [2], this relationship between force and deflection depends a lot on the sample properties but also on the apparatus geometry. Therefore, it seems necessary to revisit the modeling, especially for large deformations which are easily reached by soft biological materials. Here, we focus more on this technique once applied to living systems. Indeed, nowadays, the pivotal role of mechanics in the biological processes needs not to be demonstrated and is commonly accepted in embryogenesis, in morphogenesis, and more generally in developmental biology. Nevertheless, there is a lack of quantitative measurements and data such as the stiffness for example. This quantity itself has a much more subtle definition elaborated in the bio-mechanical field [5, 6, 7], since it strongly depends on the internal structure of living entities.

However, experimental techniques are still rather limited for micron-size systems such as cells: the classical stress/strain uniaxial apparatus is excluded at this scale, but indentation with AFM is commonly employed [8, 9, 10]. AFM seems well adapted since the indenter tip may be of order 20nm. This is not the case of glass microspheres [11] with a radius of 5μm. Another current technique concerns laser ablation, which consists in analyzing the fracture shape and which is now employed in embryogenesis (*Drosophila* [12] or *C-elegans* [13]). However, no matter which technology is used, laser ablation or indentation, one needs to revisit the elastic models for active systems, that is systems which may generate their own loadings and are also able to react to external imposed loadings [14].

On top of that, inhomogeneities such as pores cannot be discarded in biological membranes and a hole (pre-existing to the process or nucleated by it) may change drastically the measurements. Then, we focus on this aspect and propose a numerical and analytical study of indentation on a perforated membrane, with an indenter of finite size tip. To be more complete, the pre-stretch and the possibility of a soft substrate are also investigated with the objective to establish useful scaling laws at low forcing. However, the formalism of indentation is one of the classic problems of elasticity theory but also one of the most difficult and the presence of a pore adds a new step in the complexity. From the theoretical view-side, two different elastic models have emerged for indentation: the Föppl-von Kármán model (FvK, [15]) which combines plate bending and stretching undergoing moderate deflections at constant thickness, and the so-called membrane model which allows large deflections and thickness variation but ignores the bending. The advantage of the FvK is the existence of analytical solutions in ideal cases as a concentrated load but for more general loadings, such as a spherically tipped indenter, FvK modeling is a real tour de force achieved only recently, without hole [16]. In the same time, many variants of the indentation problem were considered by different groups motivated by experiments of material sciences [2, 17].

In contrast, the membrane elastic model for indentation has been elaborated quite fifty years ago, by Bhatia and Nachbar [18] for the case of a membrane undergoing large deflections in which bending moments are ignored, under a spherically tipped indenter. In a follow-up paper [19] they also consider the same problem taken a step further, namely in which the membrane under the indenter undergoes plastic deformations, so creating three coexisting zones: plastic/elastic and free zones. Although they apply linear elasticity, their formalism consists in a treatment of non-linearities for finite deformations. The rich literature on indentation becomes more limited at large deformations, when the membrane is assumed hyper-elastic. Nevertheless, let us mention the work by Yang and Hsu [20] concerning the Mooney-Rivlin model and a spherical indenter and also the work by Nadler and Steigmann [21] with the compressive Varga strain energy function [6]. However, none of these authors consider the existence of the hole even if the hole creation is considered as a possibilty in [21].

We make the choice of the membrane model with full treatment of the non-linearities in hyper-elasticity to be more adapted to our objectives. But, in our case, the difficulty is the matching of three zones: first the vicinity of the hole, second the contact zone below the tip, and finally the free membrane beginning at the indenter tip and finishing at the outer border (see the schema on right of Fig.(1). Naively, for the evaluation of the stresses, one can imagine two limits, in absence of a substrate: either the increase of the hole size by tension is such that the indenter tip can penetrate the membrane without force or the hole being too tiny, it can be ignored at low forcing and we are faced with the classical indentation process. For intermediate hole values, the hole extension and the tip penetration depth will be strongly coupled together but also with the free film scale. The amazing result is that this process which may happen gently, quite continuously, is in fact abrupt and occurs via a topological bifurcation with a jump in the position of the hole border. Such a jump in a continuous modeling is rather scarce in elasticity but reminds us the rupture of the soap-film catenoid into 2 discs when the distance of the separation increases. The topological instability in catenoid has a very long history in the theory of minimal surfaces from Euler, Lagrange, Plateau but always motivates experimental measurements since the rupture is very sensitive to any perturbation [22, 23, 24, 25]. In the domain of minimal surfaces, many other instabilities of this type have been discovered [26, 27] with formally the same explanation: physical systems described by energy minimization with coincidence of two different geometrical solutions having the same energy.

Our study then involves two aspects: first it explains this bifurcation and theoretically justifies its existence by comparing direct simulations with finite element software and the theoretical analysis deduced from our model. Second, we analyze in detail our membrane model and establish new scaling laws at low forcing (useful for the experimentalists), taking into account not only the hole and indenter tip size but also the pre-stretch and the possible existence of a substrate. When the forcing increases, the topological bifurcation is maintained in all the cases. These new scaling laws will show, if necessary, the sensitivity of the elastic response which may lead to wrong deductions

on the elastic constants of the sample.

2. Direct visualization of the transition

A uniform thin circular elastic disc of initial thickness H_0, perforated with a small hole of radius R_h at its center, is submitted to indentation. The outer border of the disc with radius R_m is rigidly fixed, and R_m will be our length unit hereafter. The indenter is made with a semi-spherical ball joined to a cylinder (see Fig.(1)) and the force F is vertical. . Choosing the neo-Hookean elasticity [5] with stiffness μ and assuming incompressibility, we perform finite-element simulations of a 2D axisymmetric model with ABAQUS software [28] and quasi-static application option. The general static solver is more appropriate for modeling highly nonlinear static problems, but because of the suspected sudden snap-through phenomena, we need the implicit dynamic solver: it captures more easily the quasi-static response and the snap-through by introducing a friction dynamics which eliminates unintended dynamical instabilities. The geometric parameters for the simulations are given in the caption of Fig.(2), the thickness being $H_0 = 0.01$, thin enough to meet the membrane condition. Around 300 eight-node axisymmetric hybrid elements (CAX8RH) are used to discretize the membrane. The boundary condition at $R_\mathrm{m} = 1$ is realized by fixing the nodes on this border. The indenter is assumed to be rigid and frictionless, and the penetration depth δ is pre-defined to mimic the displacement-loading process. Convergence of the simulations is guaranteed by comparing the results with those calculated with a refined mesh. The dynamical evolution of the membrane in response to penetration depth is shown in Fig. (2) and the video (see the Supplementary material).

In the first stage of indentation, the contact zone is confined on the spherical tip, and the hole size r_h continuously increases as well as the total elastic energy E_m given in units of $\mu H_0 R_\mathrm{m}^2$. The results obtained with ABAQUS and the membrane model (explained hereafter) coincide perfectly at low forcing, before the bifurcation (see Fig.(2)). This validates the theoretical membrane model to treat thin elastic samples at large deformations. When the penetration depth δ reaches a critical value, $\delta_\mathrm{C} = 0.448$ for our set of parameters, the membrane suddenly detaches from the spherical tip, and jumps

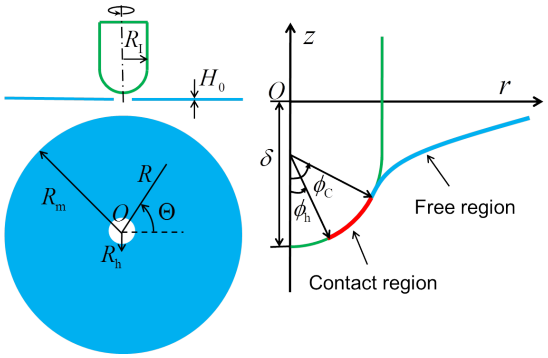

Figure 1: Sketch of the membrane indentation. On top, the geometry of the indenter, below a top view of the membrane, on right, a normal section of the deflected membrane: in green the indenter, in red the contact zone between ϕ_h and ϕ_C, and in blue the free membrane. ϕ_h and ϕ_C varies with the force F.

along the cylinder of the indenter. A schema of both stages is represented in Fig.(2), on left and right, respectively. This induces a discontinuity of both r_h and E_m, which is controlled by the indenter depth. Only the dynamic solver routine can capture this jump while the membrane model captures the unstable solutions. Fig.(2) is very similar to the classical schema of bifurcation for the catenoid, where δ can be compared to the distance between the two circular wires supporting the edges of the catenoid. r_h/R_I can be compared to the central diameter of the catenoids and our energy curve can be put into correspondence with the equivalent quantities, see Fig.(3) in Reference [25] for example. To understand better this bifurcation and because systematic simulations are time consuming and not always precise for scaling analysis, a membrane model is explained in the following section. However, one can notice the good agreement between this model which neglects the bending and the 2D model of ABAQUS (3D with axi-symmetry).

3. The theoretical non-linear elasticity model in the membrane limit

Let us define precisely the position of each point as the forcing increases, having in mind that 3 zones exist in the membrane: the hole, the zone of contact with the indenter and the free zone. The mid-surface of the membrane occupies the region between the

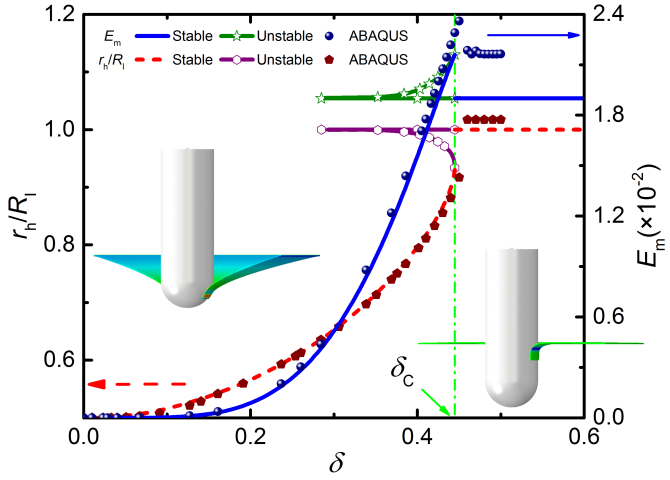

Figure 2: Numerical results: ratio between the hole and tip radius $r_{\rm h}/R_{\rm I}$ on left, and elastic energy $E_{\rm m}$ on right, versus the penetration depth δ. For this figure, $R_{\rm h} = 0.1, R_{\rm I} = 0.2, H_0 = 0.01$ and $R_{\rm m}$ is the length unit. Red dashed line (for $r_{\rm h}/R_{\rm I}$) and blue solid line (for $E_{\rm m}$) are the stable solutions of the membrane theoretical model (Section 3). Purple line with circles and green line with stars are the unstable solutions of this model. The dots on the blue continuous solid line and the red dashed line represent the simulations with ABAQUS. The jump occurs around $\delta_{\rm C} = 0.448$, which is the maximum penetration depth predicted by our numerical results. Only ABAQUS can detect the dynamical jump and new solutions are recovered after $\delta_{\rm C}$ represented by dotted horizontal segments.

hole radius $R_{\rm h}$ and the outer boundary $R_{\rm m}$ and is represented initially by the following cylindrical coordinates:

$$R_{\rm h} \leq R \leq R_{\rm m}, \quad 0 \leq \Theta \leq 2\pi, \quad Z \equiv 0 \tag{1}$$

in the initial configuration. After deformation, the mid-surface position is modified from the initial ($\mathbf{X}$) to the current configuration ($\mathbf{x} = r(R)\mathbf{e}_r + z(R)\mathbf{e}_z$) where $(\mathbf{e}_r, \mathbf{e}_\theta, \mathbf{e}_z)$ are the basis vectors in the cylindrical geometry. The hemispherical indenter tip has a radius $R_{\rm I}$ ($R_{\rm h} < R_{\rm I} < R_{\rm m}$) with $R_{\rm m} = 1$, being our length unit. Therefore, the contact between the membrane and the indenter is either limited to the small ball area (see Fig.(2), on left), or extends up to the cylindrical part of the indenter (see Fig.(2) on right), according to the loading values. Both cases are simply described in terms of the angle ϕ from the negative z-axis [29]:

$$\psi(\phi) = \begin{cases} R_{\rm I}(\sin\phi\mathbf{e}_r - \cos\phi\mathbf{e}_z) & \text{if } \phi \leq \pi/2, \\ R_{\rm I}\left(\mathbf{e}_r + (\phi - \pi/2)\mathbf{e}_z\right) & \text{if } \phi > \pi/2. \end{cases} \tag{2}$$

Considering large deformations, in the finite elasticity formalism, the principal stretches in the three directions: circumferential, tangential and normal are given by

$$\lambda_\theta = r/R, \quad \lambda_{\rm t} = \sqrt{r'^2 + z'^2}, \quad \lambda_{\rm n} = h/H_0, \tag{3}$$

where h is the current membrane thickness and $'$ denotes the differentiation with respect to R. The membrane model is valid when tension dominates for $H_0/R_{\rm m} \ll 1$ and bending can be ignored. Assuming incompressibility, the stretches verify:

$$J = \det(\mathbf{F}) = \lambda_\theta \lambda_{\rm t} \lambda_{\rm n} = 1 \tag{4}$$

and for a Neo-Hookean elasticity, the strain-energy density reads:

$$W = \frac{\mu}{2}(I_1 - 3). \tag{5}$$

where I_1 is the first invariant $I_1 = \lambda_\theta^2 + \lambda_{\rm t}^2 + \lambda_{\rm n}^2$ and μ the stiffness of the material. The Cauchy stress per unit length of the deformed membrane can be derived (see [5, 6])

$$T_\theta = \frac{H_0}{\lambda_{\rm t}} \frac{\partial W_{\rm p}}{\partial \lambda_\theta}, \quad T_{\rm t} = \frac{H_0}{\lambda_\theta} \frac{\partial W_{\rm p}}{\partial \lambda_{\rm t}}, \tag{6}$$

where $W_{\rm p}(\lambda_\theta, \lambda_{\rm t}) \equiv W(\lambda_\theta, \lambda_{\rm t}, \lambda_\theta^{-1}\lambda_{\rm t}^{-1})$. It is to be noted that the membrane modeling takes fully into account the thickness variation when the sample is stretched. Assuming there is no friction between the indenter and the membrane, the two equilibrium equations in the large deformation limits can be written as [20, 29]

$$(rT_{\rm t})' - r'T_\theta = 0, \quad \kappa_{\rm t}T_{\rm t} + \kappa_\theta T_\theta = P. \tag{7}$$

where P, a function of R, represents the pressure difference across the membrane in the normal direction. $\kappa_{\rm t}$ and κ_θ are respectively the principal curvatures in the radial and ortho-radial directions and are given by:

$$\kappa_\theta = \frac{z'}{r\sqrt{r'^2 + z'^2}}, \quad \kappa_{\rm t} = \frac{1}{r'}\left(r\kappa_\theta\right)', \tag{8}$$

where the second equation is Codazzi's equation. Notice that the principle curvatures can be written in term of the stretches λ_θ and $\lambda_{\rm t}$. In the previous section, we have yet defined the unit of energy as $\mu H_0 R_{\rm m}^2$ which means that in the following we can drop the μ coefficient from Eq.(5) and H_0 from Eq.(6).

4. Boundary and continuity conditions

The problem must be divided into two distinct regions: the contact zone of the membrane with the indenter: $R_{\rm h} \leq R \leq R_{\rm C}$, and the free region $R_{\rm C} \leq R \leq R_{\rm m}$. In the contact zone, the deformed shape follows the spherical or cylindrical surface of the indenter, depending on the strength of the forcing F. So the deformation is known but not the contact boundary and according to Eq.(2), it therefore yields

$$\begin{cases} r = R_{\rm I}\sin\phi,\ z = -\delta + R_{\rm I} - R_{\rm I}\cos\phi & \text{if } \phi \leq \pi/2, \\ r = R_{\rm I},\ z = -\delta + R_{\rm I} + R_{\rm I}(\phi - \pi/2) & \text{if } \phi > \pi/2, \end{cases} \tag{9}$$

where δ is the depth of the indenter tip. Hence, in the contact region, we can deduce the stretches:

$$\begin{cases} \lambda_{\rm t} = R_{\rm I}\phi',\ \lambda_\theta = (R_{\rm I}\sin\phi)/R & \text{if } \phi \leq \pi/2, \\ \lambda_{\rm t} = R_{\rm I}\phi',\ \lambda_\theta = R_{\rm I}/R & \text{if } \phi > \pi/2. \end{cases} \tag{10}$$

Substituting Eqs.(9,10) into Eq.(7a), it yields a piecewise second order ODE of $\phi(R)$. In the spherical area ($0 \leq \phi \leq \pi/2$), we have

$$\begin{aligned}&(3R^2 + R_{\rm I}^6\phi'^4\sin^2\phi)R^2\phi'' - 3R^3\phi' + 3R^4\phi'^2\cot\phi \\ &- R_{\rm I}^6\phi'^4\sin^3\phi\cos\phi + RR_{\rm I}^6\phi'^5\sin^2\phi = 0,\end{aligned} \tag{11}$$

and if the cylindrical part of the cylinder is also covered (with $\phi > \pi/2$):

$$(3R^3 + RR_{\rm I}^6\phi'^4)\phi'' - 3R^2\phi' + R_{\rm I}^6\phi'^5 = 0 \tag{12}$$

At the hole frontier, $R = R_{\rm h}$, in absence of surface tension, the tangential stress vanishes: $T_{\rm t} = 0$. Since also $T_{\rm n} = 0$, for an incompressible and isotropic membrane, we have then $\lambda_{\rm t} = \lambda_{\rm n} = \lambda_\theta^{-\frac{1}{2}}$. Using Eq.(10), $\phi'(R_{\rm h})$ reads:

$$\phi'(R_{\rm h}) = \frac{1}{R_{\rm I}}\sqrt{\frac{\eta}{\sin\phi_{\rm h}}}, \tag{13}$$

where $\phi_{\rm h} = \phi(R_{\rm h})$ and $\eta = R_{\rm h}/R_{\rm I}$. Finally, in the free region $R_{\rm C} \leq R \leq R_{\rm m}$, the membrane is governed by Eq.(7) with $P = 0$, which leads to some simplification for Eq.(7) (see Appendix A). The smoothness of the membrane shape imposes the continuity of r, r', z and z' on both sides of $R_{\rm C}$. At $R = R_{\rm m} = 1$, we must select a boundary condition, which will not be automatically satisfied for arbitrary $R_{\rm C}$ value. In fact, $R_{\rm C}$ is an implicit function of the border condition at R_m. Here we impose the value of the ortho-radial stretch : $\lambda_\theta = \lambda_{\rm p}(\geq 1)$ a condition which often concerns bio-membranes which are naturally in tension or "pre-stretched": $\lambda_{\rm p} > 1$ before indentation. This condition concerns cortical epithelium, see for example [11, 14, 4].

5. Matching method for $R_{\rm C}$ determination

The abundant literature on indentation demonstrates the difficulty to derive convincing solutions even when linear elasticity is adopted. In addition, most works concern full membrane without considering the possibility to enlarge a microscopic hole or eventually to nucleate a hole. Due to the importance of indentation techniques to estimate the stiffness of living specifies going from cells to tissues [9, 8], a careful numerical study is required. Indeed, the nonlinearity of the set of equations makes

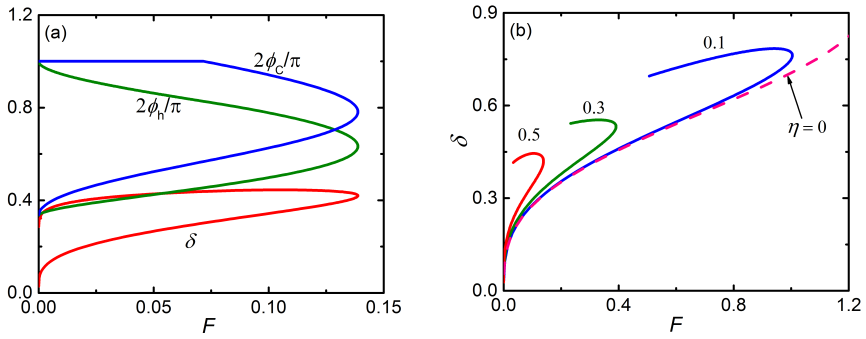

Figure 3: Numerical results for $R_{\mathrm{I}} = 0.2$. (a) The indentation depth δ, the normalized hole angle $2\phi_{\mathrm{h}}/\pi$, and the normalized maximum contact angle $2\phi_{\mathrm{C}}/\pi$ varying with the applied force F ($R_{\mathrm{h}} = 0.1$ so $\eta = 0.5$). (b) The penetration depth δ versus the force F with different initial hole size $\eta = 0, 0.1, 0.3, 0.5$. The dashed curve gives the result for $\eta = 0$, i.e. without hole.

hopeless an exact solution. All equations are now dimensionless by choosing R_{m} as length unit, μH_0 as tension unit, $\mu H_0/R_{\mathrm{m}}$ as pressure unit, $\mu R_{\mathrm{m}} H_0$ as force units and μ as energy density unit. Once ϕ_{h} is chosen leading to $\phi'(R_{\mathrm{h}})$ from Eq.(13), the nonlinear ordinary differential equation (O.D.E) of second order for ϕ (Eqs.(11, 12)) can be numerically solved. With the continuity conditions at the contact edge, the position of R_{C} gives the initial values of r and z for the free membrane, which is needed to solve the elastic deformation given by Eq.(7). However, the stretching value for $R = 1$ as the cancellation of the vertical displacement are not checked for arbitrary guess of R_{C} which will be determined by the shooting method. Once an accurate value is found after iterations, both the force and the penetration depth can be calculated:

$$F = 2\pi r T_{\mathrm{t}} \sin\phi, \quad \delta = z(1) - z(R_{\mathrm{h}}) + R_{\mathrm{I}}(1 - \cos\phi_{\mathrm{h}}), \tag{14}$$

where F is evaluated at $R = R_{\mathrm{C}}$. Additionally, the angle ϕ_{C} is also exported in order to deduce whether the membrane reaches the cylindrical surface of the indenter. If not, where $\phi(R_{\mathrm{C}}) \leq \pi/2$, we let $\phi_{\mathrm{C}} = \phi(R_{\mathrm{C}})$. Otherwise, $\phi_{\mathrm{C}} = \pi/2$. Varying ϕ_{h} and repeating the process, in fine, allows to fully study the answer of the film under indentation. The results are presented in the next section.

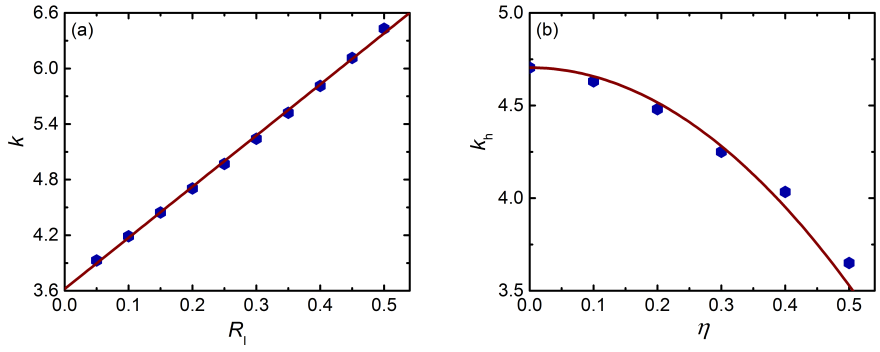

Figure 4: (a) Coefficient k (see Eq.(15)) versus $R_{\rm I}$ with $\eta = 0$, no hole in the membrane. (b) Coefficient $k_{\rm h} = k(1-\eta^2)$ versus the initial hole size parameter η for $R_{\rm I} = 0.2$. In both figures, the dots are the numerical results, and the line represents a fitting function.

6. Results

From the experimental viewpoint, indentation techniques are used to estimate either the stiffness or the residual stress/stretch remaining in the tissue [10]. It is why we orient the presentation of the results as if we were interested in measuring these quantities from an unknown membrane, once the force F is applied. Even more, in practical situations, one may ignore the existence of a tiny hole, before performing the experiment. A close comparison between results with and without hole is then essential. To simplify, in this section, we do not consider pre-stress or pre-stretch and we begin by a global description of the solutions before focussing on scaling laws.

6.1. Determination of stable and unstable solutions with increasing forcing

The three quantities: penetration length (δ), the hole ($2\phi_{\rm h}/\pi$) and contact ($2\phi_{\rm C}/\pi$) angular sizes are presented in Fig.(3a) as a function of the forcing, with $\eta = 0.5$ and $R_{\rm I} = 0.2$. The three curves exhibit a pitch-fork bifurcation with increasing F, as also shown in Fig.(2) of Section 2. For each F value, below the bound limit: $F_{\rm m}$, there are two solutions for these quantities. The lower branches of curves plotted in Fig.(3a) are perfectly recovered with the simulation of ABAQUS, by imposing displacement loading δ. But for the upper branches, it seems that one needs less force to increase the penetration depth of the indenter, which is not physical as shown by Section 2. With the

enlargement of the hole size and of the contact zone, around $F_{\rm m}$, the membrane loses its ability to resist higher indenter force, which is a sign of instability. The indenter depth δ as a function of F also shows the same bifurcation threshold which is pushed to higher values when η decreases, as shown in Fig.3(b). The dashed curve is the case for non perforated membrane $\eta = 0$, studied by [29].

The difference between these results and those of Section 2 come from the two different driving parameters: F here and δ before, which gives bound values: $F_{\rm m}$ and $\delta_{\rm C}$ respectively. Increasing δ or F gives the same path, the lower branch in Fig.(3a) but increasing forcing may cause the instability to occur earlier than increasing displacement. As a consequence $F_{\rm m}$ can always be reached experimentally but not $\delta_{\rm C}$. In most of the experimental set-ups, the force is the driving parameter as in this section. In the next section, we focus on low values of F, in the stable zone of the lower branch.

6.2. Indentation force versus penetration depth, for weak force values: possible scaling laws

The definition of a scaling law is the basis of the indentation technique. Since the experiment involves several different length scales as the size of the hole, $R_{\rm h}$, of the indenter tip $R_{\rm I}$, and of the sample (chosen as length unit) with $R_{\rm h} < R_{\rm I} < 1$, it is not easy to find universal scaling laws even for small applied force. However, we will try to establish them as much as possible, with the help of our numerical results. Without hole, at low force value, an attempt to find the penetration depth analytically has been achieved by Bathia and Nachbar [18] in linear elasticity (with $\delta \sim F$) which is not confirmed in non-linear modeling. Not surprisingly, an approach based on the FvK equations of plates [16] is in favor of a cubic law which is numerically confirmed with hyper-elastic modeling (Neo-Hookean or Mooney-Rivlin, [29]). With a hole, we expect more ambiguous results. As shown in Fig.(3b) giving the penetration depth δ versus the force F, a cubic law is verified at low δ values that we analyze carefully as a function of both competitive sizes: $R_{\rm h}$ and $R_{\rm I}$ or $R_{\rm I}$ and $\eta = R_{\rm h}/R_{\rm I}$. We propose the following:

$$F \sim k(1-\eta^2)(\delta - \delta_0)^3 \quad \text{with} \quad k = 5.52R_{\rm I} + 3.62, \tag{15}$$

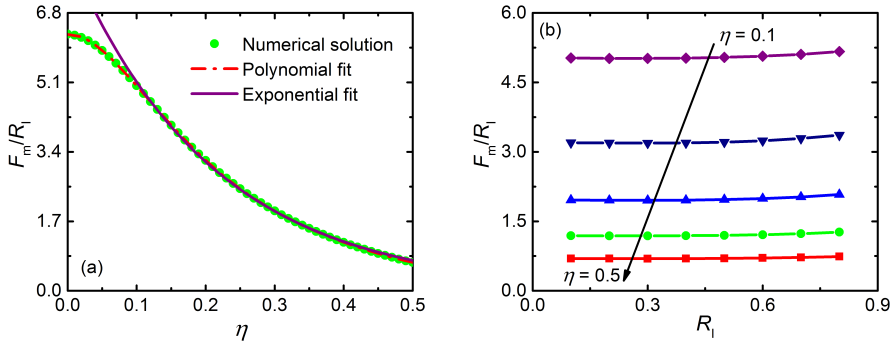

Figure 5: (a) $f_{\rm m}(\eta) = F_{\rm m}/R_{\rm I}$ versus η with $R_{\rm I} = 0.2$. Dots are numerical values of $f_{\rm m}(\eta) = F_{\rm m}/R_{\rm I}$. Two fitting functions are used and the results are shown as lines: Dashed line for a polynomial and solid line for exponential functions. (b) Variation of $F_{\rm m}/R_{\rm I}$ with $R_{\rm I}$ for several η.

where $\delta_0 = R_{\rm I}(1 - \sqrt{1-\eta^2})$, corresponding to the depth when the indenter first contacts the membrane. It is obvious to justify the cubic law (FvK nonlinear regime) as the correction $(1-\eta^2)$ which shows that the average contact pressure is the correct forcing. Increasing the initial hole size weakens the film and so requires a weaker applied force. However the coefficient k is more difficult to interpret but our numerical value 3.62 for $R_{\rm I} = 0$ is close to the one established in the FvK limit (see Appendix B) when a point load is assumed [30]. The linearity of k with $R_{\rm I}$ is demonstrated in Fig.(4a).

6.3. Scaling for the upper bound F_m

The upper bound $F_{\rm m}$ is obviously a function of both radius $R_{\rm h}$ and $R_{\rm I}$ but also of $\lambda_{\rm p}$. A discussion of $\lambda_{\rm p} > 1$ is postponed in the following section. At fixed tip radius value: $R_{\rm I} = 0.2$, Fig.(5a) displays $F_{\rm m}$ versus η. For small η, a 6-order polynomial approximation [1] can be found but as η increases, an exponential decreasing function is more adapted and useful for the following section with pre-stretch. The influence of the tip radius $R_{\rm I}$ on $F_{\rm m}$ is shown in Fig.(5b). For each line representing a fixed η, $F_{\rm m}/R_{\rm I}$ poorly varies, and the relative error is less than 2% when $R_{\rm I} \leq 0.6$. The fact that only the region closed to the indenter is affected by the indenter shape can explain

[1] $f(\eta) = (6.28 + 0.81\eta - 220.59\eta^2 + 1085.46\eta^3 - 2417.78\eta^4 + 2627.22\eta^5 - 1120.14\eta^6)$

this result so $R_{\rm I}$ is the natural length-scale. Beyond this region, the load of the indenter can be considered as a point force. Thus $F_{\rm m}/R_{\rm I}$ strongly depends on local properties and we find

$$f_{\rm m}(\eta) = F_{\rm m}/R_{\rm I} = 8.27e^{-4.82\eta}, \tag{16}$$

as demonstrated by the exponential fit in Fig.(5a).

The formula of $f_{\rm m}(\eta)$ can be used for elastic modulus measurement. We only need to know geometrical values: hole size and indenter tip, then the maximum force $F_{\rm m}$ shown by experimental data. The three values with dimension may give the shear modulus of the membrane according to:

$$\mu = \frac{F_{\rm m}}{R_{\rm I} H_0 f_{\rm m}(\eta)}. \tag{17}$$

Traditional indentation of a membrane is achieved via the determination of the $F-\delta$ curve, which obeys approximatively the relation $F = k\delta^3$ at low penetration depth δ. The coefficient k is obtained by fitting the experiment data, and then μ is estimated. If there is a possibility to make a hole with a controlled size, our measurement method may have several advantages. First, we only need to record the maximum $F_{\rm m}$, and this is more accurate. $F_{\rm m}$ is obtained under large δ, which is less affected by external interference. Second, we can directly obtain μ from Eq.(17), without any fitting of experiment data. The fundamental experimental challenge is of course to make a hole on a membrane and to increase the force rather slowly to maintain the stability of the lower branch.

7. Tense membrane indentation

Biological membranes are not free of stresses and pre-stretch or stress affects a lot the nonlinear elasticity. One may think that the previous analysis, in particular, the topological bifurcation may disappear under pre-stretch. As shown by Fig(6), it is absolutely not the case: the pitch-fork bifurcations for δ versus F are maintained always with the existence of an upper bound: $F_{\rm m}$. Of course numerical values depend on $\lambda_{\rm p}$ but not the global schema. Looking more carefully, the zone of low forcing is significantly modified. So in the area of interest for experimentalists, we can claim

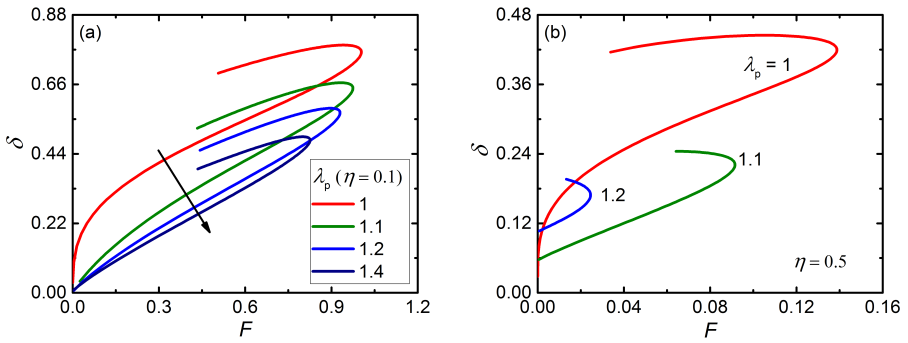

Figure 6: Penetration depth-force relationships for several pre-stretch values with $\eta = 0.1$ in (a) and $\eta = 0.5$ in (b), $R_{\rm I} = 0.2$.

that pre-stretch cannot be discarded. Therefore, we follow the same steps as before, beginning with the regime of weak force, then focussing on the values of $F_{\rm m}$.

7.1. Scaling at low forces under pre-stretch

For the indentation of a perfect membrane with pre-stretch, several papers [17, 31, 32] quote a formula without demonstration:

$$F = \pi T_{\rm pre}\delta + \alpha_0 \frac{\delta^3}{\lambda_{\rm p}^4}, \tag{18}$$

where $T_{\rm pre}$ is the uniform tension induced by the pre-stretch, $T_{\rm pre}$. This formula can be intuitively understood as the addition of the two terms (tension and compression) in the non-linear regime of FvK [15]. It contains the linear term (with the pre-stress) and the classical cubic term. For finite indenter radius, different variants with a logarithmic correction $R_{\rm I}$ can be found in [2, 33]. In particular, Vella *et al.* [2] point out that the linear term only concerns the small δ limit evaluated with a point force in the FvK model. Since no asymptotic results are known for the transition going from small to large δ, they propose the empirical result:

$$F = \frac{2\pi}{\ln(\lambda_{\rm p}/R_{\rm I})} T_{\rm pre}\delta + \left(3.65 + 11.07\left(\frac{R_{\rm I}}{\lambda_{\rm p}}\right)^{\frac{2}{3}}\right)\frac{\delta^3}{\lambda_{\rm p}^4} \tag{19}$$

This form is intuited for a cylindrical indenter with a flat tip in contact with the membrane, the radius of the contact zone being fixed to $R_{\rm I}$. We compare Eq.(19) (solid lines)

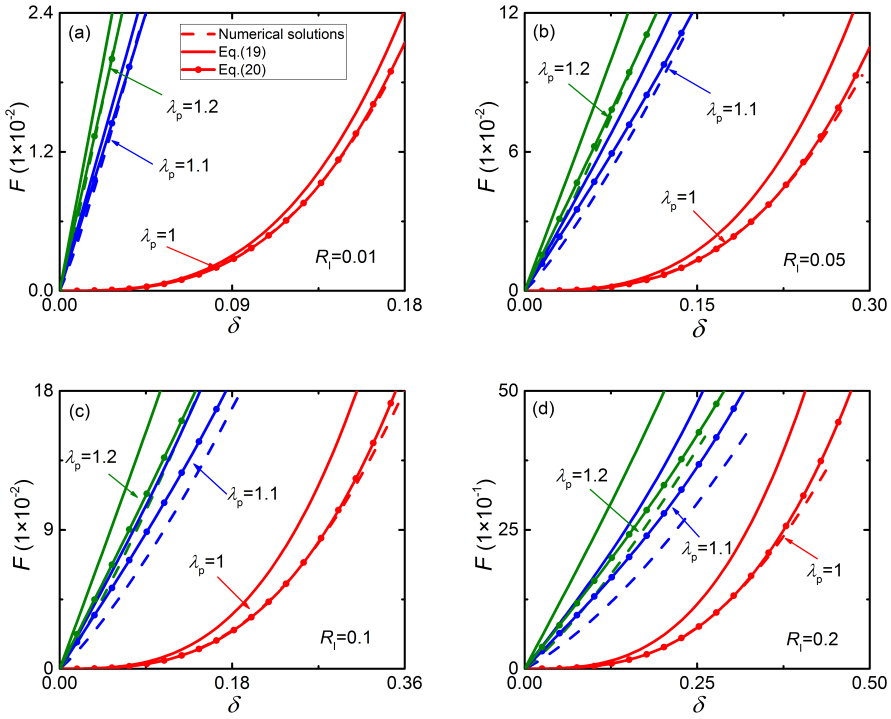

Figure 7: Force F versus the indenter depth δ as the pre-stretch λ_p varies: comparison of the numerical results with 2 possible scaling laws according to Eqs.(19,20) for different indenter radii. (a)$R_{\rm I} = 0.01$, (b) $R_{\rm I} = 0.05$, (c) $R_{\rm I} = 0.1$ and (d) $R_{\rm I} = 0.2$. The dashed line represents the numerical solutions. The scaling laws according to Eq.(19) (resp. Eq.(20)) are shown as solid line (resp. as solid line with circles). Notice that the solid line with circles is closer to the dashed line so Eq.(20) is a better representation.

with our numerical solutions (dashed lines) in Fig.(7), for $R_{\rm I} = 0.01, 0.05, 0.1, 0.2$ and $\lambda_{\rm p} = 1, 1.1, 1.2$. Although it is the best approximation up to now, the results of Eq.(19) are not consistent with our geometry: the force is overestimated (see Fig. (7)). This proves the sensitivity of the geometry of the indenter tip. To limit the discrepancy, we modify the Vella-Davidovitch formula for the first term and replace the coefficient of the last term of Eq.(19) by our very similar relation k in Eq.(15) which reads:

$$F = \frac{2\pi}{\ln(\lambda_{\rm p}^6/R_{\rm I})} T_{\rm pre}\delta + \left(3.62 + 5.52\frac{R_{\rm I}}{\lambda_{\rm p}}\right)\frac{\delta^3}{\lambda_{\rm p}^4}. \qquad (20)$$

Comparison of both Eq.(19) and Eq.(20) with our numerical results is displayed in Fig.(7). Eq.(20) shows a significant improvement when $R_{\rm I} = 0.01, 0.05$, but it cannot

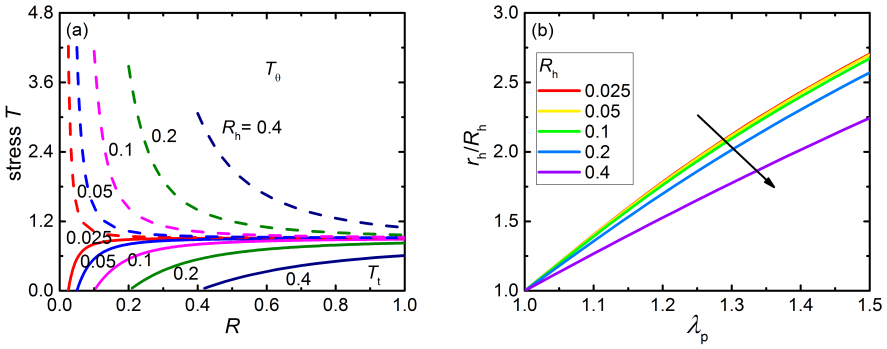

Figure 8: Results with no indentation under pre-stretch. In (a) radial $T_{\rm t}$ (continuous lines) and ortho-radial T_θ (dashed lines) tensions as a function of R for different values of the hole radius $R_{\rm h} = 0.025, 0.05, 0.1, 0.2, 0.4$ and fixed $\lambda_{\rm p} = 1.5$. In (b) the stretch of the hole: $r_{\rm h}/R_{\rm h}$ as a function of the pre-stretch $\lambda_{\rm p}$ for different initial size values $R_{\rm h}$.

match well with the numerical data for $R_{\rm I} = 0.2$. Therefore, there is still a challenge to find a proper solution for a indenter with spherical tip in contact with a pre-stretched perforated membrane, even when the applied forces are very small.

7.2. Scaling for force bound under pre-stretch

In this Section, we try to establish the maximal force $F_{\rm m}$. Imposing $\lambda_{\rm p}$ increases the original size of the hole and changes the initial stress distribution around the hole. Thus it has a strong influence on the indentation process. First, we study the hole size and stress distribution of the membrane without indentation. Fig.(8a) shows the distribution of the in-plane stresses $T_{\rm t}$ and T_θ in the membrane for a variety of $R_{\rm h}$ with $\lambda_{\rm p} = 1.5$. When $R_{\rm h} \leq 0.1$, both stresses vary sharply at small distances from the hole and then join together giving $T_{\rm t} \sim T_\theta$ giving an isotropic state. But when $R_{\rm h} > 0.1$, this local property disappears gradually. Fig.(8b) shows the variation of $r_{\rm h}$ with $\lambda_{\rm p}$. Only when $R_{\rm h} \leq 0.1$, $r_{\rm h}$ is linearly dependent on $R_{\rm h}$.

Next, we study the influence of $\lambda_{\rm p}$ under indentation with fixed indenter radius $R_{\rm I} = 0.2$. Two η values are chosen: 0.1 and 0.5. Once the pre-stretch $\lambda_{\rm p}$ increases, the relation between F and δ changes from cubic to linear within the regime of weak force, and $F_{\rm m}$ decreases as shown in Fig.(6). When the hole size under pre-stretch becomes

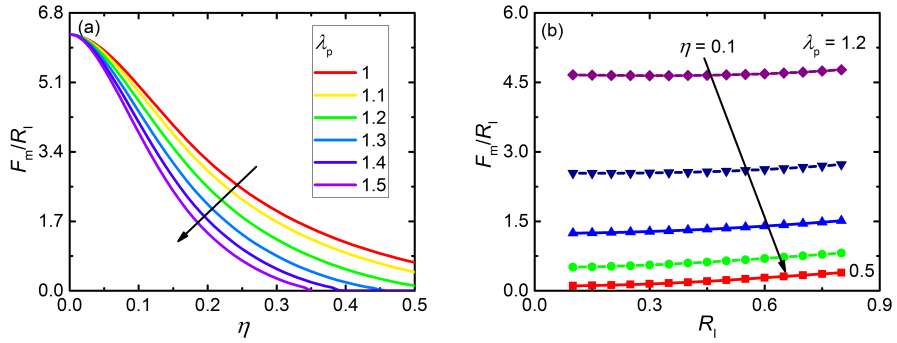

Figure 9: (a) The maximal force $F_{\rm m}/R_{\rm I}$ at fixed $R_{\rm I} = 0.2$, under different pre-stretch values. (b) $F_{\rm m}/R_{\rm I}$ as a function of $R_{\rm I}$ at fixed pre-stretch $\lambda_{\rm p} = 1.2$.

larger than the indenter, F vanishes which means that there is no resistance for indenter penetration, see Fig.(6b).

Similar to previous section, we can extract $F_{\rm m}$ with fixed $R_{\rm I} = 0.2$ and plot it in Fig.(9a). The influence of $R_{\rm I}$ on $F_{\rm m}$ with $\lambda_{\rm p} = 1.2$ is also plotted in Fig.(9b). Unfortunately, $F_{\rm m}$ is no longer varying linearly with $R_{\rm I}$. Thus the general form of $F_{\rm m}$ is:

$$F_{\rm m} = \Pi(R_{\rm I}, \eta, \lambda_{\rm p}). \tag{21}$$

The total coupling among three parameters is a very tough problem. We admit some constraints to decouple. The straightforward method is to limit the hole size $R_{\rm h} \leq 0.1$, so the assumption of local stress distribution is preserved. Then we check Fig.(9b), and find that $F_{\rm m}$ is linearly dependent on $R_{\rm I}$, approximatively. Therefore,

$$F_{\rm m} = R_{\rm I}\mathcal{F}(\eta, \lambda_{\rm p}). \tag{22}$$

Using the data in Fig.(9a), the fitting function has the form:

$$\mathcal{F}(\eta, \lambda_p) = (8.27 + a_0\Lambda_{\rm p})e^{(b_0\Lambda_{\rm p} - 4.82)\eta} + c_0\Lambda_{\rm p}, \tag{23}$$

where $\Lambda_p = \lambda_p - 1$, $a_0 = 2.99, b_0 = -4.23, c_0 = -1.93$, see Fig.(10a).

In experiments, most of the time, it is not possible to find the free stress state of the membrane. For indentation experiments with pre-stretch, we can only measure the

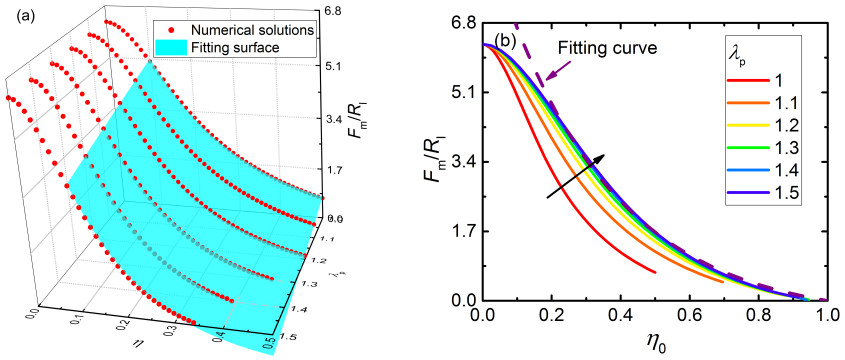

Figure 10: (a) The surface fit deduced from Fig.(9a) represented by Eqs.(22,23). (b) Maximum force versus $\eta_0 = r_{\rm h}^0/R_{\rm I}$.

radius $r_{\rm m}^0$, thickness h^0 and the hole size $r_{\rm h}^0$ of the membrane under an unknown pre-stretch $\lambda_{\rm p}$. Using the data from Fig.(9a), we can obtain the maximum force varying with $\eta_0 = r_{\rm h}^0/R_{\rm I}$ shown in Fig.(10b). The parameter $F_{\rm m}/R_{\rm I}$ expressed with dimension is

$$\frac{F_{\rm m}}{\mu H_0 R_{\rm I}} = \frac{F_{\rm m}}{\mu \lambda_{\rm p}^2 h^0 R_{\rm I}}. \tag{24}$$

With increasing $\lambda_{\rm p}(\geq 1.3)$, the lines join together, which means that the difference of $F_{\rm m}/R_{\rm I}$ between $\lambda_{\rm p}$ with the same η_0 is very small. This indicates that for "large" pre-stretch values:

$$\frac{F_{\rm m}}{\mu \lambda_{\rm p}^2 h^0 R_{\rm I}} \sim \Gamma(\eta_0) \approx 0.48(e^{-2.99(\eta_0-1)} - 1), \tag{25}$$

where the quantity $\mu\lambda_{\rm p}^2$ can only be deduced from experimental results. Thus, the shear modulus μ and pre-stretch $\lambda_{\rm p}$ can not be obtained separately by only fitting experimental data under "large" pre-stretch.

8. Membrane with foundation

Most of biological membranes are supported by an elastic substrate which can be either the extra-cellular matrix, the interior of the cell or of embryos. In this last part, we simply represent this possibility by an elastic foundation, such as a collection of springs, according to the Winkler model. The spring force applied on the membrane

per unit surface is given by $K_s z$, and the force direction is always perpendicular to the membrane surface. Thus, the second equation of Eq.(7) needs to be modified by adding $K_s z$ in the right-hand side, K_s being scaled by $\mu H_0/R_m^2$. Additionally, the indentation force which was given by Eq.(14) is also modified and, once evaluated at $R = R_C$:

$$F = 2\pi r T_t \sin\phi + \frac{1}{3} K_s \pi R_I^2 \big(2R_I(1-\cos^3\phi) + 3(\delta - R_I)\sin^2\phi\big). \qquad (26)$$

The Winkler model is easy to implement in our formulation, unlike the juxtaposition of two nonlinear connected elastic samples. However, now, the numerical process requires two initial guess values for δ and R_C instead of one, which leads to numerical instabilities. From Eq.(7) and Eq.(11) with proper initial conditions given at $R = R_h$, the values of λ_θ and z at $R = 1$ can be obtained. We then iterate on δ and R_C to meet the boundary conditions $\lambda_\theta = \lambda_p$ and $z = 0$ at $R = 1$.

For the indentation of a perfect membrane supported by an elastic foundation, the force-penetration depth results for $R_I = 0.2$ with several K_s are illustrated in Fig.(11a). We propose the fitting function:

$$F = g_s \delta + k\delta^3, \qquad (27)$$

where the coefficient g_s is a function of R_I and K_s. For $R_I = 0.2$, g_s varying with K_s is plotted as circular points in Fig.(11b). In order to obtain the function $g_s(R_I \equiv 0.2, K_s)$, we use two types of fitting functions, linear $g_s = 0.365K_s$ and quadratic $g_s = -0.101K_s^2 + 0.406K_s$, shown as solid lines in Fig.(11b). Considering biological systems, the membrane can be either stiffer than the inside gel (for example, the interior of *C.elegans*) or softer (the substrate contains fibers). The linear relation is enough, if $K_s \leq 0.5$. Further, g_s varying linearly with R_I for fixed $K_s = 0.2, 0.4$ are shown in Fig.(11c), and then we obtain the following formula

$$g_s = K_s(0.59R_I + 0.25). \qquad (28)$$

Several results of perforated membranes are presented in Fig.(12). In the range of K_s values used here, the main tendency is maintained.

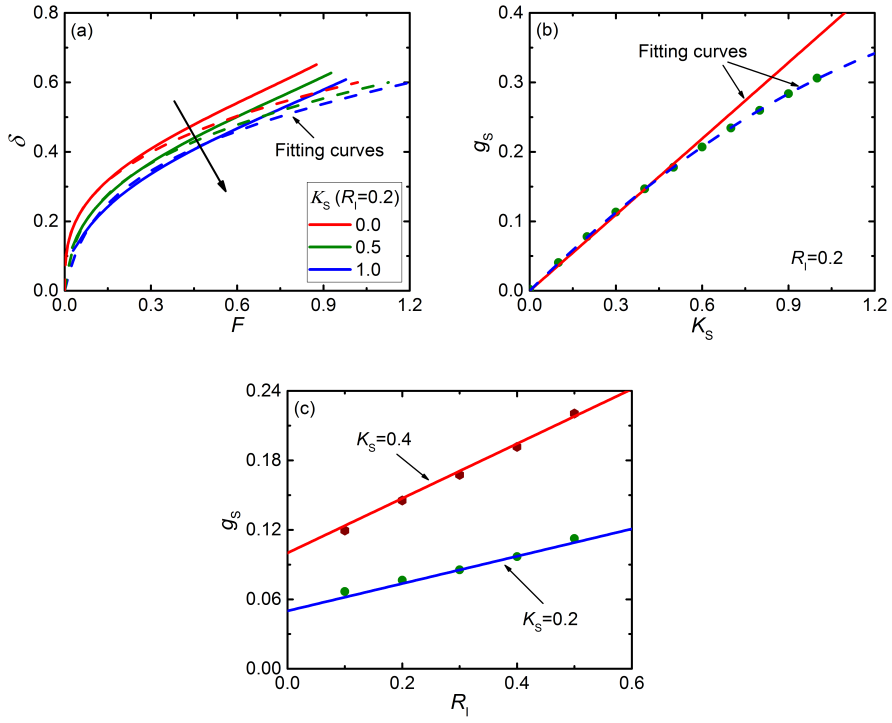

Figure 11: (a) $\delta - F$ curve with several foundation stiffness $K_{\rm s}$, where $R_{\rm I} = 0.2$. The numerical results are plotted as solid lines, and the fitting curves are plotted as dashed lines. (b) The coefficient $g_{\rm s}$ versus $K_{\rm s}$, according to Eq.(27). (c) $g_{\rm s}$ versus $R_{\rm I}$ with fixed $K_{\rm s} = 0.2$ and 0.4.

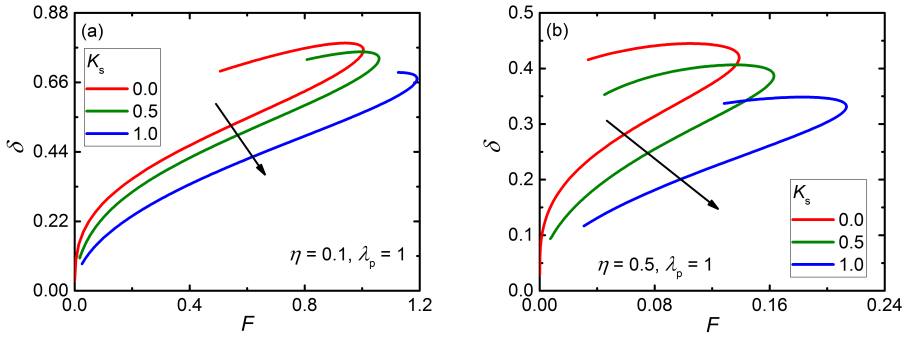

Figure 12: $\delta - F$ curve with several foundation stiffness $K_{\rm s}$ with $R_{\rm h} = 0.02$ for (a) and $R_{\rm h} = 0.1$ for (b), $R_{\rm I} = 0.2$.

Table 1: Stretch values at the bifurcation for different hole radius

R_{h}	0.01	0.02	0.03	0.04	0.05	0.06	0.07	0.08	0.09	0.1
λ_θ	10.73	6.31	4.69	3.88	3.36	2.86	2.55	2.28	2.06	1.86
λ_{n}	0.305	0.398	0.462	0.508	0.546	0.591	0.626	0.662	0.697	0.732

First line, on top: the size hole R_{h} compared to the membrane radius, second line: corresponding ortho-radial stretch, λ_θ, third line: the compressive stretch λ_{n} in the thickness of the membrane

9. Conclusion

In this work, we systematically revisit the theory of indentation of a perforated membrane in situation mostly relevant to biophysics although other domains may also be concerned. We fully take into account the large deformation limit which concerns elastic samples with a low shear modulus. Our purpose is first to establish relevant scaling laws for experimentalists who want to access the elastic properties of membranes. We demonstrate that the existence of a tiny hole or the nucleation of the hole strongly affects the traditional cubic law, well accepted in the field. In fact, this scaling valid for low forcing concerns a perfect isolated membrane, free of stretch before indentation, a situation not often encountered in practice. In addition, there is no clear definition of the limit "low forcing" since these membranes are hyper-elastic and may obey different hyper-elasticity. Here, restricting on Neo-Hookean elasticity, we show that this scaling law depends a lot, in a non-trivial way, on the following factors: hole-size, tip-radius, pre-stretch and substrate elasticity, requiring each time a specific study.

One may be concerned by the validity of the Neo-Hookean approach employed here. Indeed, it has been shown in [29] that this model may lose its validity when the stretches λ_{t} and λ_θ exceeds 3.5 for an indenter radius: $R_{\mathrm{I}} = 0.2$. The fact that, in the center of a membrane without hole, $\lambda_{\mathrm{t}} = \lambda_\theta$ imposes a stretching value λ_n for the thickness given by $\lambda_{\mathrm{n}} = \lambda_\theta^{-2} = 1/3.5^2 \sim 0.08$ which means a significant compression in the membrane below the indenter tip and fixes the limit of validity of the Neo-Hookean approach. It turns out that this effect is released by the existence of a hole

which modifies the elastic field in its vicinity giving at the periphery, $\lambda_{\rm t} = \lambda_{\rm n} = \lambda_\theta^{-1/2}$. The largest stretch value is not at the tip but at the bifurcation point of Fig. (1) where we find $\lambda_\theta = r_{\rm h}/R_{\rm h} = 1.86$ and a compressive stretch $\lambda_n \sim 0.733$. So the strains have reasonable values and surely fall in the range of validity of the neo-Hookean modeling. We also check λ_θ for a variety of hole sizes $R_{\rm h}$ fixing all other parameters to the same values as in Fig.(1) (see also Table 1). Not surprisingly, only tiny holes with $R_h < 0.01$ (or $\eta < 0.05$), are responsible for large stretches, λ_θ exceeding 3.5^2. So, except in these limiting cases, most of our results are still in the range of validity of the neo-Hookean elastic energy.

But in our opinion, the major result is the existence of a topological bifurcation where the main characteristics of the system under study become unstable as the forcing increases and jump to a different value. It is the case for the hole-size, the penetration depth, the contact zone between indenter tip and membrane, all of them becoming discontinuous. This bifurcation is demonstrated in two ways: theoretical membrane modeling and 3D finite element dynamical simulations (ABAQUS), which by the way, coincide perfectly. This topological change presents similarities with the catenoid minimal surfaces when the support is pulled apart. It is also true that these two systems are controlled by minimization of an energy, in the static case. The amazing result is that this bifurcation is robust and it is maintained whatever the physical modelings investigated here. It is probably because it corresponds to a geometrical bifurcation always encountered when a hole exists.

10. Supplementary material

A video for the indentation process of a perforated membrane is available online, for this article.

11. Acknowledgments

The authors acknowledge the support of ANR (Agency Nationale de la Recherche) under the contract MECATISS (ANR-17-CE30-0007) and under the contract EPIMORPH (ANR-18-CE13-008), the National Natural Science Foundation of China (Grants

No. 11772276 and No.11402217). We express our sincere appreciation to Simon P. Pearce (University of Manchester) for sharing his code [29].

Appendix A.

In this section, we give the main steps leading to the membrane treatments in the free part. One simplification comes from the absence of forcing F or P, but the deformation is not known. In Eq.(7) with $P = 0$, we have

$$T_\theta = -\frac{\kappa_\mathrm{t} T_\mathrm{t}}{\kappa_\theta}, \quad (rT_\mathrm{t})' + r'\frac{\kappa_\mathrm{t} T_\mathrm{t}}{\kappa_\theta} = 0. \tag{A1}$$

Using Codazzi's equation(8), the second equation of Eq.(A1) can be written as

$$\begin{aligned} 0 &= \frac{1}{rT_\mathrm{t}}\left[(rT_\mathrm{t})' + \frac{(r\kappa_\theta)' T_\mathrm{t}}{\kappa_\theta}\right] \\ &= \frac{(rT_\mathrm{t})'}{rT_\mathrm{t}} + \frac{(r\kappa_\theta)'}{r\kappa_\theta} \end{aligned} \tag{A2}$$

Then,

$$T_\mathrm{t} = \frac{A}{r^2\kappa_\theta}, \tag{A3}$$

where A is a constant. In fact, A is the normalized force $F/(2\pi)$ [29]. From Eq.(6), we have

$$T_\mathrm{t} = \frac{F}{2\pi r^2 \kappa_\theta} = \frac{1}{\lambda_\mathrm{t}\lambda_\theta}\left(\lambda_\mathrm{t}^2 - \frac{1}{\lambda_\mathrm{t}^2\lambda_\theta^2}\right). \tag{A4}$$

Substituting Eq.(A3) into Eq.(A1) and with Eq.(6), it reads

$$T_\theta = -\frac{\kappa_\mathrm{t}}{\kappa_\theta}\frac{1}{\lambda_\mathrm{t}\lambda_\theta}\left(\lambda_\mathrm{t}^2 - \frac{1}{\lambda_\mathrm{t}^2\lambda_\theta^2}\right) = \frac{1}{\lambda_\mathrm{t}\lambda_\theta}\left(\lambda_\theta^2 - \frac{1}{\lambda_\mathrm{t}^2\lambda_\theta^2}\right). \tag{A5}$$

Appendix B.

For the membrane without hole and pre-stretch,

$$F \sim k\delta^3, \tag{B1}$$

at lower forcing, where the coefficient k is a function of R_I. The fitting range for k is chosen as that the stretch λ_t at the membrane center is $1 \leq \lambda_\mathrm{t} \leq 1.1$. The results are

shown as dots in Fig.(4a), from which k varies linearly with R_{I}. Thus we use linear fitting and obtain

$$k \approx d_1 R_{\mathrm{I}} + d_0, \tag{B2}$$

where $d_1 = 5.52$, $d_0 = 3.62$.

From this approximate k, it yields a constant d_0, which is corresponding to the limit case of the indentation under point load. From paper [30], the coefficient k for point load case is

$$k \approx \frac{3}{\left(1.05 - 0.146 \times 0.5 - 0.158 \times 0.5^2\right)^3} = 3.65, \tag{B3}$$

which is very close to our constant 3.62.

Considering the effects of the hole, the force has the form

$$F \sim k_{\mathrm{h}} (\delta - \delta_0)^3, \tag{B4}$$

where $\delta_0 = R_{\mathrm{I}}(1 - \sqrt{1-\eta^2})$, and $\eta = R_{\mathrm{h}}/R_{\mathrm{I}}$. Fixing $R_{\mathrm{I}} = 0.2$, we can have k_{h} for each η by numerical calculation. The results are shown in Fig.(4b), where the dots are the numerical results and the function with the following form matches well with numerical results,

$$k_{\mathrm{h}} \approx k(1 - \eta^2). \tag{B5}$$

Therefore, for general case, we have

$$F = (d_1 R_{\mathrm{I}} + d_0)(1 - \eta^2)(\delta - \delta_0)^3. \tag{B6}$$

References

[1] B.J. Briscoe, L. Fiori and E. Pelillo, Nano-indentation of polymeric surfaces,J. Phys. D: Appl. Phys. 31 (1998) 2395 doi.org/10.1088/0022-3727/31/19/006

[2] D. Vella, B. Davidovitch, Indentation metrology of clamped, ultra-thin elastic sheets, Soft Matter. 13 (2017) 2264-2278. doi:10.1039/c6sm02451c.

[3] D. Vella, A. Ajdari, A. Vaziri, A. Boudaoud, The indentation of pressurized elastic shells: From polymeric capsules to yeast cells, J. R. Soc. Interface. 9 (2012) 448–455. doi:10.1098/rsif.2011.0352

[4] A. Sanzeni, S. Katta, B.C. Petzold, B.L. Pruitt, M.B. Goodman, M. Vergassola, Tissue mechanics and somatosensory neural responses govern touch sensation in C. elegans, BioRxiv(under Peer Rev. (2018). doi:10.1101/471904.

[5] R.W. Ogden, Non-linear Elastic Deformation, Dover Publications and Ellis Horwood, New York, 1984.

[6] G.A. Holzapfel, Nonlinear solid mechanics: a continuum approach for engineering, wiley, Chichester, 2000.

[7] A. Goriely, The Mathematics and Mechanics of Biological Growth, Springer, 2017. doi:10.1007/978-0-387-87710-5.

[8] J. Lathia, S. Mack, E. Mulkearns-Hubert, C. Valentim, J. Rich, Cancer stem cells in glioblastoma, Genes Dev. 26 (2015) 758. doi:10.1101/gad.261982.115.tumors.

[9] S. Digiuni, A. Berne-Dedieu, C. Martinez-Torres, J. Szecsi, M. Bendahmane, A. Arneodo, F. Argoul, Single cell wall nonlinear mechanics revealed by a multi-scale analysis of AFM force-indentation curves, Biophys. J. 108 (2015) 2235-2248. doi:10.1016/j.bpj.2015.02.024.

[10] R. Malgat, F. Faure, A. Boudaoud, A Mechanical Model to Interpret Cell-Scale Indentation Experiments on Plant Tissues in Terms of Cell Wall Elasticity and Turgor Pressure, Front. Plant Sci. 7 (2016) 1351. doi:10.3389/fpls.2016.01351.

[11] A.L. Eastwood, A. Sanzeni, B.C. Petzold, S. Park, B.L. Pruitt, M.B. Goodman, Tissue mechanics govern the rapidly adapting and symmetrical response to touch, Proc. Natl. Acad. Sci. 112 (2015) E6955-E6963. doi:10.1073/pnas.1604954113.

[12] P.C. Shivakumar, P.F. Lenne, Laser Ablation to Probe the Epithelial Mechanics in Drosophila, in: Drosophila, Humana Press, New York, NY, 2016: pp. 241-251. doi:10.1016/B978-0-12-804066-9.00024-9.

[13] T.T.K. Vuong-Brender, M. Ben Amar, J. Pontabry, M. Labouesse, The interplay of stiffness and force anisotropies drives embryo elongation, Elife. 6 (2017) e23866. doi:10.7554/elife.23866.

[14] M. Ben Amar, P.Q. Qu, T.T.K. Vuong-Brender, M. Labouesse, Assessing the Contribution of Active and Passive Stresses in C. elegans Elongation, Phys. Rev. Lett. 121 (2018) 268102. doi:10.1103/PhysRevLett.121.268102.

[15] L.D. Landau, E.M. Lifshitz, Theory of Elasticity, Pergammon, 1986.

[16] C. Jin, A. Davoodabadi, J. Li, Y. Wang, T. Singler, Spherical indentation of a freestanding circular membrane revisited: Analytical solutions and experiments, J. Mech. Phys. Solids. 100 (2017) 85-102. doi:10.1016/j.jmps.2017.01.005.

[17] A. Castellanos-Gomez, V. Singh, H.S.J. Van Der Zant, G.A. Steele, Mechanics of freely-suspended ultrathin layered materials, Ann. Phys. 527 (2015) 27-44. doi:10.1002/andp.201400153.

[18] N.M. Bhatia, W. Nachbar, Indentation of an Elastic Membrane by a spherical indenter, Int. J. Non. Linear. Mech. 3 (1968) 307-324.

[19] N.M. Bhatia, W. Nachbar, Finite indentation of elastic-perfectly plastic membranes by a spherical indenter, AIAA J. 6 (1968) 1050-1057. doi:10.2514/3.4672.

[20] W.H. Yang, K.H. Hsu, Indentation of a circular membrane, J. Appl. Mech. 38 (1971) 227-230. doi:10.1115/1.3408747.

[21] B. Nadler, D.J. Steigmann, Modeling the indentation, penetration and cavitation of elastic membranes, J. Mech. Phys. Solids. 54 (2006) 2005-2029. doi:10.1016/j.jmps.2006.04.007.

[22] M. Ben Amar, P.Patrício da Silva, N. Limodin, A. Langlois, M. Brazovskaia, C. Even, I.V. Chikina, P. Pieranski, Stability and vibrations of catenoid-shaped smectic films, Eur. Phys. J. B. 3 (1998) 197-202. doi:10.1007/s100510050303.

[23] S.A. Cryer, P.H. Steen, Collapse of the soap-film bridge: quasistatic description, J. Colloid Interface Sci. 154 (1992) 276-288. doi:10.1016/0021-9797(92)90101-Q.

[24] F. Müller, R. Stannarius, Collapse of catenoid-shaped smectic films, Europhys. Lett. 76 (2006) 1102-1108. doi:10.1209/epl/i2006-10397-8.

[25] M. Ito, T. Sato, In situ observation of a soap-film catenoid - A simple educational physics experiment, Eur. J. Phys. 31 (2010) 357-365. doi:10.1088/0143-0807/31/2/013.

[26] A. Boudaoud, P. Patrício, M. Ben Amar, The helicoid versus the catenoid: Geometrically induced bifurcations, Phys. Rev. Lett. 83 (1999) 3836-3839. doi:10.1103/PhysRevLett.83.3836.

[27] R.E. Goldstein, J. McTavish, H.K. Moffatt, A.I. Pesci, Boundary singularities produced by the motion of soap films, Proc. Natl. Acad. Sci. 111 (2014) 8339-8344. doi:10.1073/pnas.1406385111.

[28] ABAQUS, Analysis Theory manual, 2009.

[29] S.P. Pearce, J.R. King, M.J. Holdsworth, Axisymmetric indentation of curved elastic membranes by a convex rigid indenter, Int. J. Non. Linear. Mech. 46 (2011) 1128-1138. doi:10.1016/j.ijnonlinmec.2011.04.030.

[30] U. Komaragiri, M.R. Begley, J.G. Simmonds, The Mechanical Response of Free-standing Circular Elastic Films Under Point and Pressure Loads, J. Appl. Mech. 72 (2005) 203. doi:10.1115/1.1827246.

[31] C. Lee, X. Wei, J.W. Kysar, J. Hone, Measurement of the Elastic Properties and Intrinsic Strength of Monolayer Graphene, Science 321 (2008) 385-388.

[32] G. López-Polín, C. Gómez-Navarro, V. Parente, F. Guinea, M.I. Katsnelson, F. Pérez-Murano, J. Gómez-Herrero, Increasing the elastic modulus of graphene by controlled defect creation, Nat. Phys. 11 (2015) 26-31. doi:10.1038/nphys3183.

[33] D. Norouzi, M.M. Müller, M. Deserno, How to determine local elastic properties of lipid bilayer membranes from atomic-force-microscope measurements: A theoretical analysis, Phys. Rev. E. 74 (2006) 061914. doi:10.1103/PhysRevE.74.061914.